Potential of multiple injection strategies implementing the after shot and optimized with the design of experiments procedure to improve diesel engine emissions and performance

POTENTIAL OF MULTIPLE INJECTION STRATEGIES IMPLEMENTING THE AFTER SHOT AND OPTIMIZED WITH THE DESIGN OF EXPERIMENTS PROCEDURE TO IMPROVE DIESEL ENGINE EMISSIONS AND PERFORMANCE.

d'Ambrosio, S., and Ferrari, A.*

Energy Department – Politecnico di Torino

C.so duca degli Abruzzi, 24, 10129, Torino, Italy.

1. ABSTRACT.

The potential of the after-injection versus engine-out emissions, combustion noise and brake specific fuel consumption has been evaluated for a Euro 5 diesel engine with a reduced compression ratio (16.3:1). The engine has been fueled with conventional diesel fuel. In particular, the effects of injection strategies that feature either pilot and after-injection shots, or double-pilot and single-after injection shots, have been assessed experimentally, in the presence of high *EGR* fractions. Calibrations with triple and quadruple injection schedules have been optimized by means of a design of experiments procedure. The performance of the thus calibrated propulsion system has been compared with data from a previously optimized double injection schedule, characterized by a retarded main injection timing in order to intensify the premixed combustion. The experimental data refer to different steady-state working conditions that are representative of passenger car engine applications over the European homologation cycle. In-cylinder analyses of the pressure, heat release rate, temperature and emissions have been performed in order to have a better understanding of the effects of the implemented injection strategies on engine performance.

The substitution of the pilot- main injection schedule in the higher part-load zone of the *NEDC* region with a triple injection, featuring both pilot and after shots, has led to lower NO_x and higher soot, while fuel consumption remains almost the same. In general, the *EGR* trade-off soot-NO_x, *bsfc*-NO_x, *HC*-NO_x and *CO*-NO_x curves do not change to any significant extent when an after shot is added to the pilot-main injection train. Reductions in the combustion noise, which depend on the changes in the pilot injection parameters that result from the design of experiments procedure, can also be obtained, as a consequence of the addition of the after-injection to the pilot-main injection schedule. Pilot-pilot-main-after strategies guarantee improved NO_x-soot and *bsfc*-NO_x *EGR* trade-off curves at medium to high loads and at

* Corresponding author e-mail address: alessandro.ferrari@polito.it.

low to medium speeds, compared to both pilot-pilot-main and pilot-main-after strategies, and allow combustion noise to be diminished significantly.

Keywords: after injection; design of experiments; partial premixed charge compression ignition engines.

Highlights:

- The benefits of after injections are evaluated in a low-compression ratio Euro 5 diesel engine.
- Triple and quadruple injection schedules are compared with pilot-main and pilot-pilot-main strategies.
- The potential of after injections is examined in the higher part of the *NEDC* load zone.

2. INTRODUCTION

The fuel injection strategy can play an important role in simultaneously reducing passenger car diesel engine emissions [1, 2, 3, 4] and combustion noise [5], without neglecting fuel consumption targets. In other words, a multiple injection strategy, adopted to replace a single fuel injection shot with multiple discrete fuel injection events of reduced size, can easily be implemented using Common Rail (*CR*) systems, equipped with the modern injectors [6, 7]. These injectors can control small injected fuel quantities, despite pressure waves, and guarantee superior flexibility in the management of the dwell time, in order to fulfil Euro 5 and Euro 6 standards.

There are two primary multiple injection modes: the first elemental mode, which uses pilot injection, can be implemented by injecting an amount of fuel prior to the main injection (the pilot injected mass is small in conventional diesel combustion systems, but can also be significant in low temperature combustion strategies [2]), while the other employs after-injection, which consists of a small amount of fuel being injected separately, at the end of the main injection. The benefits and effects of pilot injections on emissions, combustion noise (*CN*) and fuel consumption have been evaluated and discussed in [8]. The focus of this work is on the exploitation of optimized after-injection in multiple injection strategies, in order to improve engine out emissions and in-cylinder performance. From this point of view, after-injection is efficient in reducing the soot engine-out emissions [9], which can be up to 40% lower than in the single injection case [10]. In general, after-injections can oxide part of the unburned fuel and a decrease in *CO*, *HC* and *PM* engine-out emissions is obtained [11]. The benefits increase when mixing is difficult, i.e. at medium to high loads and under high *EGR* conditions when the utilization of in-cylinder air is critical [12, 13].

After-injections have also been proposed as a means of reducing turbocharger lag during engine transients, since the pressure and the temperature of the exhaust gas leaving the cylinder can be raised significantly [14]. This makes the turbocharger accelerate more quickly and allows the aggressive increase in the injection quantity to be started sooner, since the fuel quantity growth must follow the increase in the air supply in order to avoid high soot during transients.

Finally, after-injections can be applied to raise the diesel oxygen catalyst (*DOC*) temperature above its light-off temperature after a cold start and post injections[1] can then be supplied to raise the exhaust temperature even further [15, 16].

Soot emissions are affected remarkably by the duration of the main injection. In fact, an important source of smoke emissions exists in diesel engines at the end of main combustion, because both the equivalence ratio and local in-cylinder temperature are high [17]. In particular, when long main-injection durations are considered, even a small reduction in the energizing time of the main injection can provide significant soot benefits [18]. The shortened temporal length of the main injection in multiple injection schedules featuring an after shot, produces less soot. Furthermore, the contribution of soot from after-injected fuel, if planned correctly, can be lower than in the case in which the after-injected fuel is included in the main injection [19]. When after-injection fuel is introduced into the combustion chamber, the local equivalence ratio is lower than it is at the end of the main injection without after-injection. In fact, the fuel is not injected at the same location since the piston is moving [20]. An enhanced air-fuel mixing occurs, due to the presence of two separate smaller combustion events [10], according to a split flame type behaviour [17]. Furthermore, improved particulate oxidation occurs later on in the combustion cycle, because of the increased in-cylinder bulk temperatures during the expansion stroke [21].

An optimum main-after *DT* value, which depends on the after injected mass, exists for the optimization of the interaction between the combustion of the main injection and the combustion of the after injection, as well as for the subsequent minimization of the soot produced in the overall combustion [22]. In fact, if the *DT* is too short, the after fuel is injected into the regions where the combustion of the main fuel takes place. The atomized fuel spray lacks oxygen because the after-injection entrains the burned gases. As a result, combustion progresses gradually, causing a low heat release peak and the slow combustion rate during diffusion combustion causes the smoke emissions to increase. In these cases, the after-injection produces additional soot rather than oxidizing the previously formed soot, as a consequence of the main injection. On the other hand, if the after pulse is too late, the combustion of the after fuel occurs at excessively reduced temperatures and, although the soot production, which is due to the after injected fuel is limited (this production becomes virtually null for an after injection into surrounding gases with lower temperatures than 700 K [23]), the after-shot is once again unable to properly oxidize the soot produced during the main combustion. The greatest smoke reduction is achieved when the start of the after-injection is phased within a tiny window of the main diffusive flame [20] in order to guide the after-fuel into the squish volume [24]. The optimum *DT* value is in the 600÷1000 μs range for passenger cars (instead the optimum after injection timing is in the 30-40° *CA ATDC* for delayed main injection timings in heavy duty engines [25, 24]) and a constant *DT*, which corresponds to the optimum value, is usually applied in the *ECU* maps for a medium speed and load range. As the mass of the after-injected fuel increases,

the main-after *DT* that minimizes the soot emissions, tends to augment. The quantity of the after injection is also a trade-off: if this quantity is too small, there is no significant effect of the after-shot and, if the fuel quantity is too high, the higher fuel mass has to burn in a high equivalence ratio environment [20]. The optimum after injection quantity is in the 1.5÷3 mm^3 range (around 15-20% of the total fuel mass in heavy duty engines [24]), i.e. small enough to prevent a quasi-steady diffusion flame from being established [23].

Main-after injection strategies also affect NO_x, *bsfc* and *CO* engine-out emissions. The presence of an after injection can make the last part of the *HRR* curve of a pilot-main combustion rise faster than in the case without an after-injection, even though all the fuel is introduced earlier in the latter case [17]. The smaller the size of the after injection, the higher the acceleration of the final stage of combustion. Therefore, if a small after-injection is placed close to the main injection, the combustion process can conclude earlier than in the without the after-shot case. This can explain why the engine efficiency can be higher and the engine exhaust temperature can be lower when an early after-injection is used [26]. If the after-injection is phased close to the main injection, the combustion barycentre moves toward the *TDC* and the flame temperatures rise, thus leading to higher level of NO_x emissions and lower *CO* emissions than in the absence of the after shot. If the after-injection timing occurs sufficiently far from the main injection, the NO_x emissions improve compared to the without the after-injection case, whereas the fuel economy undergoes penalties for larger after injections, which lead to higher *bsfc* reductions. Finally, the after-injection spray, for after injection timings at about 40° *CA ATDC*, reaches the wall of the liner, creating wall-wetting and thus rapidly increasing *HC* and *bsfc* [27].

When heavy *EGR* rates (*EGR* fractions around 60%) are applied to control NO_x, most of the after injection cases generate an increment in the soot and in *HC* and *CO*, because the after injected fuel cannot burn well due to the poor oxygen concentration and delayed ignition [28]. This effect is in contrast with the main effect of after injection under moderate *EGR* rates (EGR fractions in the 25÷40 range). However, a small amount of fuel, injected in an after-injection with a short dwell time with respect to the main injection, can reduce fuel consumption, soot, *HC* and *CO*, compared to single injections, even for heavy *EGR* rates [29].

An after-injection can be effectively combined with one or more pilot shots in order to develop sophisticated injection strategies for the control of engine-out emissions, combustion noise and fuel consumption, in the medium load and speed area of a low-compression ratio engine. Contributions on this topic are available in the literature [27, 30, 31], but lack of information is still present about the impact of optimized calibrations featuring the after injection.

In the present work, the potentialities of triple and quadruple injection schedules are evaluated and the results on emissions and performance, in the presence of an after-shot, are compared with those referring to pilot-main and pilot-pilot-main injection strategies, at different steady-state engine working conditions. All the triple and quadruple injection engine calibrations have been optimized with the design of experiment (*DoE*) technique, and the pilot-main injection

engine calibration represented a state-of-the-art double injection calibration. This comparison between optimum calibrations therefore allows the effective benefits of the after injection to be assessed. Furthermore, the after injection is implemented in the presence of high *EGR* rates, whereas most of the researches on the after shot are conducted under low or moderate *EGR* conditions [32].

3. EXPERIMENTAL SETUP AND ADOPTED INEJCTION STRATEGIES.

The experimental tests have been carried out on the highly-dynamic test bench, installed at the Politecnico di Torino ICEAL (IC Engines Advanced Laboratory) and equipped with an 'ELIN AVL APA 100' cradle-mounted AC dynamometer. An 'AVL KMA 4000' has been used to continuously meter fuel consumption, with a reading accuracy of 0.1% over a 0.28-110 kg/h range. Furthermore, an 'AVL AMAi60' system, made up of different analyzer trains, has been applied to measure the engine-out gaseous raw emissions of *HC*, NO_x and *CO*, as well as the CO_2 levels in the intake manifold, in order to evaluate the *EGR* rate. Finally, an AVL 415S smokemeter allows the engine-out soot emissions to be evaluated in the exhaust gases.

The experimental data have been analyzed with the support of a previously developed three-zone combustion model [33]. Ordinary differential mass and energy conservation equations have been applied to the fuel, unburned gas and burned gas zones and have been solved numerically, on the basis of the experimental in-cylinder pressure. The model allows the temperatures of the three zones to be predicted as functions of the crank angle. Furthermore, thermal and prompt *NO* mechanisms are implemented in the code, according to the Zeldovich and Fenimore submodels, respectively. The soot formation is modeled [42] by means of an expression that considers the mean air-fuel ratio over the combustion period, while the soot oxidation rate is modeled using an empirical law, based on the temperature of the burned gas zone.

Table 1 reports the scheme and the main features of the investigated Euro 5 passenger car diesel engine, fueled with conventional diesel oil. This engine has been equipped with a *DOC* and a diesel particulate filter, while no aftertreatment device has been designed to reduce the NO_x emissions. The engine has been fully instrumented with piezoresistive pressure transducers and thermocouples, in order to measure the pressure and temperature in the intake, exhaust and *EGR* lines of the engine. A high-frequency piezoelectric transducer has been installed in the glow-plug seat to measure the pressure time-histories of the gases in the combustion chamber of one cylinder. Another piezoresistive transducer has been used to detect the pressure levels in the inlet runner of the same cylinder and thus to reference the in-cylinder pressure.

The implemented triple (both pilot-pilot-main and pilot-main-after) and quadruple (pilot-pilot-main-after) engine calibrations have been optimized by means of the design of the experiments (*DoE*) statistical technique [8]. The

following parameters were considered as the most relevant input variables for the procedure: rail pressure (p_{Rail}), swirl actuator position (Sw), dwell times between consecutive injections (DT_{Pil1} between the pilot 1 and main shots, DT_{Aft} between the main and after shots and DT_{Pil2} between the pilot 2 and pilot 1 shots in quadruple injection strategies, where pilot 1 is the closest shot to the main injection and pilot 2 the furthest shot from the main injection), main injection timing (SOI_{Main}), the injection quantities in each pilot or after shot (q_{Pil1}, q_{Aft} and q_{Pil2} in quadruple injection strategies), the inducted air per stroke and per cylinder (m_a) and the boost pressure (p_{Boost}) at high load.

An engine working-point, evaluated as representative of engine application to a passenger car over the new European driving cycle, has been considered a key point. The following key-points were selected for the considered engine (n [rpm]×$bmep$ [bar]): 1500×2, 1500×5, 2000×2, 2000×5, 2500×8, 2750×12 and idle.

For instance, Tables 2-4 report (second column) the parameter levels that were considered in the variation lists for the optimizations of the *pMa* injection schedule, at the 2000×5 and 2750×12 key-points, and of the *ppMa* strategy, at the 1500x5 key-point. The center and the extreme values of the levels that were considered for each parameter were chosen on the basis of preliminary measurements. An appropriate number of levels was selected in order to obtain accurate results with a reasonable number of tests for each variation list. The quantity of fuel in the main injection is set by the test-bench control system, in order to guarantee the *bmep* value, and is therefore not present as a parameter in the variation list. The inducted air (m_a), measured by means of the air mass flowmeter, was considered in the variation lists, instead of the *EGR* ratio. The p_{Boost} pressure only appears in the variation list of 2750x12 since has a lower influence for the other key points, which Tables 2 and 4 refer to. Furthermore, the simultaneous control of p_{Boost} and *EGR* can constitute a problem in the presence of high X_{EGR} values, which occur at key points 2000x5 and 2750x12.

The preliminary variation list of each considered key-point was obtained using the Matlab Model-Based Calibration toolbox, setting a V-optimal type design of experiments, which minimizes the prediction error variance, and a full factorial series, as the candidate set, on the basis of the levels shown in Tables 2-4. The final variation lists were made up of 120-150 tests for each considered key point, including replications of the central point (defined by the center value of the levels for each parameter).

Once the variation list tests had been carried out, on the engine, it was possible to obtain quadratic models of the output variables as functions of the input variables and of their interactions. The engine-out specific NO_x, *CO*, *HC* and soot emissions, the *bsfc* and the *CN* were considered as the output variables. Different targets can be introduced for the output variables in order to select the best set of values for the input variables at each key point, that is, the optimized engine calibration. In the present work, the optimization strategy for the triple and quadruple injection calibrations, based on the *DoE*, has been aimed at minimizing the NO_x emissions and at reducing the combustion noise, compared to the pilot-main injection baseline calibration, which was originally implemented in the ECU provided by the engine

178 *OEM*. In fact, the goal is to avoid the application of any aftertreatment device for the NO_x emissions. The presence of a
179 *bsfc*-NO_x trade-off constituted a constrain to the simultaneous reduction in *bsfc* and NO_x and a slight increase in *bsfc* has therefore
180 been accepted
181 Tables 5-7 show the reference values of the output variables for the pilot-main injection strategy and the constraints
182 used for the optimization of the triple and quadruple injection strategies, which Tables 2-4 refer to. The optimized
183 values of the input variables, calculated by means of the DoE procedure, are reported in the third column of Tables 2-4.
184 *EGR* trade-offs have been performed in the neighborhood of the baseline calibration points for the double, triple and
185 quadruple injection strategies, in order to compare not only the baseline points of the different calibrations, but the
186 complete EGR curves. The considered engine calibrations are characterized by elevated *EGR* mass fractions (
187 $X_{EGR} = \dot{m}_{EGR}/(\dot{m}_a + \dot{m}_{EGR})$), within the 45-55% range.

188 ## 4 PILOT-MAIN-AFTER INJECTION STRATEGIES.

189 If reference is made to the pilot-main (*pM*) and pilot-main-after (*pMa*) baseline calibrations at *bmep*=5 bar and *n*=2000
190 rpm, the addition of an after injection, featuring a relatively late timing (SOI_{after}≈20° *CA ATDC*) with respect to the
191 main injection, leads to a significant reduction in the NO_x emissions (cf. Fig. 1, the contoured triangle and circle
192 symbols) and in *CN* (cf. Fig. 2, the contoured triangle and circle symbols), while *bsfc*, soot, *HC*, and *CO* (cf. Figs. 3-6,
193 the contoured triangle and circle symbols) become worse. However, the penalties on soot, *HC* and *CO* are acceptable,
194 since the engine is equipped with both a *DOC* and a particulate filter. In general, *CN* improves by about 1.2÷1.5 dB for
195 the different X_{EGR} values in the *pMa* case (Fig. 2), while the *bsfc*-NO_x, soot-NO_x, *HC*-NO_x and *CO*-NO_x *EGR* trade-off
196 curves (Figs. 3-6) coincide for the *pM* and the *pMa* strategies.
197 Figures 7-10 compare the crankshaft angle based distributions of the *HRR*, T_b, NO_x and soot for the baseline calibrations
198 of the *pM* and the *pMa* strategies (as previously mentioned, the *pMa* baseline calibration is the output of the *DoE*
199 optimization procedure). Since the timing adopted for the after-injection is delayed, the after combustion (Fig. 7) takes
200 place under low in-cylinder pressure and gas temperatures (Fig. 8), and the peak burned gas temperature also reduces
201 for the *pMa* strategy, due to the higher X_{EGR} value. Furthermore, the residence time of the burned gases at higher
202 temperatures than 1950 K is longer for the *pM* calibration (Fig. 8). Finally, the proximity of the pilot combustion to the
203 main combustion and the increased X_{EGR} value can lead to richer stoichiometric equivalence ratios for the *pMa* strategy
204 at the start of the main combustion. All of these circumstances induce increased NO_x emissions for the *pM* strategy,
205 compared to the without after-injection case (Fig. 9), because the thermal NO_x increase with the value of the flame
206 temperature during the diffusive portion of combustion and are only produced in the presence of sufficient O_2
207 concentrations in the post-flame zones [34]. The reduced *DT* between the pilot and main injection in the *pMa* strategy

allows a softer transition between the pilot and main combustion (the *HRR* peak of the main combustion is higher for the *pM* case), and is therefore beneficial in suppressing combustion noise.

As far as the *PM* is concerned (Fig. 10), the low-temperature combustion of the after-injected fuel does not generally oxidize the previously formed soot. Furthermore, the presence of heavy *EGR* rates prevents the after-injected fuel from burning well, because of a lack of oxygen concentration. As a consequence, the after injection on its own produces increments in the quantity of the particulate matter, and this is proved by the change in rate, which occurs at $\theta \approx 385°$ *CA* along the soot curve of the *pMa* strategy. The higher soot level obtained for the *pMa* strategy is also the result of the lower premixed portion of its main combustion: in fact, the *HRR* peak pertaining to the main combustion in Fig. 7 is higher for the *pM* strategy than for the *pMa* one.

As already mentioned, the *pMa* calibration selected in the present case has had the aim of reducing the NO_x emissions and combustion noise [35]; the soot emissions are controlled by the retarded SOI_{Main} ($\approx 2°$ *CA ATDC*) and, above all, by the diesel particulate filter (cf. also Table 5).

The *HC* and *CO* emissions in Figs. 5 and 6 are higher for the *pMa* baseline calibration point because of the retarded after combustion [36, 10], which causes incomplete oxidation, and because of the possible presence of a greater number of over-rich mixture zones at the start of combustion of the main injected fuel (cf. also Table 5).

Finally, the delayed after-injection (cf. *MFB50* values in Fig. 11) raises the temperature at the engine exhaust (cf. T_{exh} in Fig. 12) for the *pMa* baseline calibration. This leads to a larger thermal energy loss at the engine exhaust and thus explains the slight deterioration in the *bsfc*, shown in Fig. 3, and also found in [37]. On the other hand, the higher T_{exh} values can be exploited to reduce the turbocharger lag during engine transients.

Figures 13-20 refer to n=2500 rpm and *bmep*=8 bar. The main difference in the *HRR* diagrams in Fig. 13, compared to those in Fig. 7, concerns the position of the pilot injection, which occurs earlier for the *pMa* strategy. Furthermore, the rail pressure level is $p_{rail} \approx 1200$ bar at this key-point for the *pM* calibration, whereas it reduces to $p_{rail} \approx 1125$ bar for the *pMa* calibration (a higher injection pressure promote a better air-fuel mixing [38]). No pilot combustion occurs in the *pMa* case, and the role of the main injection is therefore to trigger fuel ignition, which can cause interference between the pilot injected fuel flames and the main injection (the soot increases significantly in Fig. 17 for the *pMa* case).

The NO_x and *CN* are lower for the baseline point of the *pMa* calibration (cf. Fig. 20), and the causes of the improved NO_x are again the decreased residence time of the burned gas at very high temperatures, the reduced p_{nom} value and the relatively high local equivalence ratios in the $360° \ CA < \theta < 390° \ CA$ range (cf. Figs 14 and 15). The soot and *CO* emissions are better for the *pM* injection baseline calibration (cf. Figs. 17 and 19) and the reasons for this are the same as those provided for the previously analyzed engine key-point. However, unlike for n=2000 rpm and *bmep*=5 bar, the soot-NO_x and *CO*-NO_x trade-offs become slightly worse for the *pMa* strategy, and the *CN*-NO_x curve of the *pMa*

strategy is no better than that of the *pM* strategy. The general improvement in the *HC* emissions that results from the application of the *pMa* injection schedule (cf. Fig. 18) is related more to the absence of the pilot combustion (the main injection triggers the ignition of the pilot injected fuel for the *pMa* strategy and this probably reduces the occurrence of overleaning) or to the reduced rail pressure level than to the addition of the after shot.

The *bsfc*-NO_x trade-off, the soot-NO_x trade-off, the *CO*-NO_x trade-off and the *CN*-NO_x *EGR* curve for n=2750 rpm and *bmep*=12 bar are reported in Figs. 21-24. The *pMa* calibration improves the soot-NO_x and the *CO*-NO_x trade-offs, but penalties are incurred in *bsfc* (cf. also Table 6). The *HC*-NO_x trade-off also improves for the *pMa*, but the *HC* values are lower than 0.1 g/kWh for both strategies and are therefore not a cause of concern. The *CO* emission levels in Fig. 23 are not critical either.

5 PILOT-PILOT-MAIN-AFTER INJECTION STRATEGIES.

Double *pM* and triple *ppM* injection strategies have been compared with *pMa* and *ppMa* strategies at medium load and speed conditions.

Figures 25-29 report the experimental results at *bmep*=5 bar and n=1500 rpm for the different calibrations. The triple injections (either *ppM* or *pMa*) do not improve the *bsfc*-NO_x (Fig. 25), soot-NO_x (Fig. 26) *HC*-NO_x (Fig. 27) or *CO*-NO_X (Fig. 28) *EGR* trade-offs, compared to the *pM* calibration. The *CN*-NO_x curve (cf. Fig. 29) does not change either when passing from the *pM* to the *ppM* or *pMa* injection schedules.

No discrepancy can be observed between the results concerning *CN* in Fig. 29 and those reported in Figs. 2, which refer to a similar working condition. In fact, the higher the engine speed at fixed *bmep*, the higher the combustion noise levels [39]. Furthermore, Fig. 30 shows that the pilot and main combustion events are clearly distinct for both the *pM* and the *pMa* baseline calibration points, unlike the events shown in Fig. 7, where the transition from the pilot to the main combustion was softer for the *pMa* strategy and this explained the lower *CN* (the difference between the main combustion *HRR* peaks of the *pM* and *pMa* calibrations is greater in Fig. 7 than in Fig. 30). Finally, the ignition delay of the main injected fuel in Fig. 30 is slightly longer, and the *HRR* peak attributed to the pilot combustion is higher for the *pMa* schedule than for the *pM* one; both these results are physically consistent with the *CN* increase detected for the *pMa* calibration [40].

In short, the after-injection only seems to have an indirect impact on the management of combustion noise. The addition of the after shot to an injection train can produce relevant changes in the optimized *DoE* calibration. In particular, the presence of the after injection can modify certain pilot injection parameters, such as pilot injection quantity and timing. These parameters can influence the interaction between the pilot mixture field and the main injection, that is, the way the main injection interferes with the ignition process of the pilot mixture and influences its combustion process, and

thus can significantly affect the combustion noise [40]. In general, in addition to the described interaction, hydraulic interference between the pilot and main injections may also occur [41]. In fact, the different sets of pilot injection masses and timings can generate different pressure values in the injector delivery chamber at the SOI_{main} instant, due to the variability in the pressure wave dynamics. Therefore, the velocity at which the needle opens the nozzle during the main energizing time can vary for the different calibrations and this can have an appreciable impact on the noise. In general, the higher the needle velocity at the beginning of the main injection, the higher the combustion noise. This hydraulic effect can be remarkable when pilot injections with lower *DT* than 500 μs are implemented, [6], but it is not significant for the pilot-main *DT* considered in Fig. 30, (the enlargement in Fig. 30 shows smaller differences than 20% in the injected flow-rate slope).

The *ppMa* calibration allows the *bsfc*-NO_x and the *CN*-NO_X *EGR* curves in Figs. 25 and 29 to be improved (cf. Table 7). A slight benefit can also be observed in the management of the soot-NO_x trade-off (cf. Fig. 26). On the other hand, no benefits can be observed for the quadruple injection with respect to the *HC-NO* (Fig. 27) or to the *CO*-NO_X (Fig. 28) *EGR* trade-offs, compared to *pM* and *ppM* strategies.

Figures 31-33 report the burned gas temperature, the NO_x and the soot in-cylinder angular distributions for the baseline calibration points of the four considered injection strategies. These diagrams, together with the *HRR* traces, complete the in-cylinder numerical analysis. Even though *ppMa* features the highest T_b values (Fig. 31), the NO_x engine-out emissions are minimized (Fig. 32). This behavior is probably due to the equivalence ratio distributions within the cylinder.

Part of the fuel injected in the later-pilot injection burns during the main injection event in the *ppMa* baseline calibration (cf. Fig. 30), and a larger amount of rich mixture (with $\phi \geq 2$) results in the fuel spray of the main injection (the global O_2 concentration is also minimum for the *ppMa* case). As a consequence, the NO_x emissions diminish. For the same reason, a great peak of soot can be seen in Fig. 33 for the *ppMa* case, although the energizing time of the main injection is reduced, and the high T_b values and the appropriate timing of the after-injection, with respect to the main shot ($DT \approx 600$ μs), promote a greater oxidation of the soot generated during the main combustion. The *pM* baseline calibration shows lower interference between pilot combustion and the main injection and employs the lowest X_{EGR} value. As a result, a soot level minimum can be found at the engine exhaust (cf. Fig. 33). On the other hand, the high T_b values encountered during diffusive combustion could explain the great increase in the NO_x over the $370° \, CA < \theta < 390° \, CA$ range for this strategy. Furthermore, a significant production of NO_x also occurs for the *pM* strategy during the diffusive portion of pilot-injected-fuel combustion, i.e., over the $360° \, CA < \theta < 365° \, CA$ range.

In the case of the *ppM* calibration, the higher rail pressure nominal value, i.e. p_{rail}≈750 bar instead of p_{nom}≈620 bar, which is applied to all the other strategies at 1500x5, is responsible for the relatively high NO_x engine-out emissions that can be observed in Fig. 32.

As far as the pilot injection is concerned, the highest temperatures of the unburned gases (cf. Fig. 31 for θ<350° *CA*), the reduced ignition delay of the fuel injected in the earlier pilot shot, and the major interference between the combustion event pertaining to the earlier pilot injection and the fuel injected in the later pilot shot, are the reasons for the augmented soot production over the 350° *CA*<θ<365° *CA* interval in the *ppMa* case (cf. also Table 7).

The less steep pattern of the *HRR* curve for the *ppMa* calibration is the reason for the general lower combustion noise level in Fig. 29. This *HRR* pattern is induced by the reduced entity of the premixed combustion, as a consequence of the more pronounced interaction between the oxidation of the fuel, which is injected in the later pilot injection shot, and the main injection.

6 CONCLUSIONS.

Multiple injection strategies featuring an after shot have been compared with pilot-main and pilot-pilot-main injection strategies in a low-compression ratio Euro 5 diesel engine, in order to evaluate the possible benefits in engine-out emissions, combustion noise and fuel consumption, at medium to high loads and at low to medium speeds.

All the triple and the quadruple injection strategies considered in this work have been optimized by means of a *DoE* procedure: this aspect is relevant because it allows the effective benefits of the after injection to be assessed. *EGR* trade-offs have been carried out around the baseline calibration points obtained from the *DoE* and around the *pM* injection calibration. The latter represented the state-of-the-art double injection calibration of the considered engine technology. Experimental tests have been conducted in a dynamometer cell and different steady-state key-points, which were representative of the medium-high part load zone of the *NEDC* for a passenger car engine application, have been considered. The experimental analysis has been supported by numerical results, which were derived from the application of diagnostic combustion models, on the basis of the measured trace of the in-cylinder pressure time history. The main outcomes concerning the effects of the after injection on pilot-main injection strategies with postponed main injection timings are reported synthetically hereafter.

- At medium to high loads and medium speeds, *DoE* optimized calibrations featuring after-injections with delayed timings (10-15° *CA ATDC*) can improve engine-out NO_x emissions, compared to the *pM* baseline calibration, because the after-injections take place at low in-cylinder pressures and gas temperatures. However, since the applied DT_{Aft} values are relatively large, soot emissions grow and *bsfc* is slightly higher than in the case of the *pM* baseline

calibration. Furthermore, *CO* engine-out emissions tend to become worse for the *pMa* baseline calibration, due to the reduced temperatures of the after combustion.

- The soot-NO_x, *bsfc*-NO_x and *CO*-NO_x trade-offs of the engine calibration that employs the after injection do not change significantly, compared to those referring to a *PCCI* late strategy featuring a pilot-main injection schedule. Furthermore, the addition of the after-injections does not show any clear effect on the *HC*-NO_x trade-off, which can either improve or become worse, depending on the considered *bmep* and *n* values. However, the *HC* engine-out emissions are not a concern at medium speed and medium to high loads, which represent the typical working conditions of the after injection strategy.
- After-injection only seems to have only an indirect impact in the management of combustion noise. The addition of the after-shot to an injection train can produce relevant changes in a *DoE* optimized calibration. In particular, the presence of an after-injection can modify certain pilot injection parameters, such as the pilot injection quantities and timings. These parameters can influence the interaction between the pilot mixture field and the main injection, i.e., the way the main injection interferes with the ignition process of the pilot mixture and influences its combustion process. All this can have a significant effect on combustion noise. As proof of the complex correlation between the after-shot and combustion noise, a comparison between the *pM* and *pMa* experimental data has shown that, for the *pMa* calibration, the *CN* generally improves by 2 *dB* at *bmep*=5 bar and *n*=2000 rpm, but generally deteriorates by 1 dB at *bmep*=5 bar, *n*=1500 rpm and at *bmep*=12 bar, *n*=2750 rpm.
- The application of *ppMa* injection schedules at medium load and speed leads to improvements in the soot-NO_x, *bsfc*-NO_x trade-offs, compared to the *pM* and *ppM* strategies. Furthermore, *CN* reduces significantly, while the *CO*-NO_x trade-offs do not become worse. The presence of four injection shots leads to an increased flexibility in the management of the different constraints and in particular in the design of the best interaction between the pilot injection combustions and the main injection. A combination of *ppMa* strategies and high *EGR* rates is therefore recommended in low-compression ratio engines featuring delayed main injection timing.

7 NOMENCLATURE.

bmep	brake mean effective pressure
bsfc	brake specific fuel consumption
CA	crankshaft angle degree
CN	combustion noise
DOC	diesel oxygen catalyst
DoE	design of experiments

357	*DT*	dwell time
358	*ECU*	electronic control unit
359	*EGR*	exhaust gas recirculation
360	*HC*	unburned hydrocarbons
361	*HRR*	heat release rate
362	m_a	fresh air mass per stroke and per cylinder
363	$\dot{m}_a$	fresh air mass flow-rate
364	$\dot{m}_{EGR}$	exhaust gas recirculation mass flow-rate
365	*MFB50*	angle at which 50% of the combustion mixture has burned
366	*n*	engine speed
367	NO_x	nitrogen oxides
368	$O_{2\,int}$	oxygen volume concentration
369	p_{Boost}	boost pressure
370	p_{int}	pressure in the intake manifold
371	p_{cyl}	in-cylinder pressure
372	p_{rail}	nominal rail pressure level
373	*PCCI*	premixed charge compression ignition
374	*PM*	particulate matter
375	*q*	injected quantity (volume)
376	*TDC*	top dead center
377	*SOI*	electrical start of the injection
378	*Sw*	swirl actuator position
379	T_b	burned gas temperature
380	*TDC*	top dead center
381	X_{EGR}	mass fraction of exhaust gas recirculation
382	ϕ	equivalence ratio
383	λ	relative air-to-fuel ratio
384	θ	crankshaft angle in the simulations
385	***Subscripts***	
386	*Main*	main injection

Pil1 pilot 1 injection

Pil2 pilot 2 injection

Aft after injection

8 REFERENCES.

[1] Mohan, B., Yang, W., and Chou, S. K., 2013, "Fuel injection strategies for performance improvement and emissions reduction in compression ignition engines — A review", *Renewable and Sustainable Energy Reviews*, vol. 28, pp. 664-676.

[2] Fang, Q., Fang, J., Zhuang, J., and Huang, Z., 2012, "Influences of pilot injection and exhaust gas recirculation (*EGR*) on combustion and emissions in a HCCI-DI combustion engine", *Applied Thermal Engineering*, vol. 48, pp. 97-104.

[3] Suh H.K., 2011, "Investigations of multiple injection strategies for the improvement of combustion and exhaust emissions characteristics in a low compression ratio (CR) engine", *Applied Energy* 88 pp. 5013–5019. doi:10.1016/j.apenergy.2011.06.048.

[4] Zheng M., Kumar R., 2009, "Implementation of multiple-pulse injection strategies to enhance the homogeneity for simultaneous low-NOx and -soot diesel combustion". *International Journal of Thermal Sciences* 48 pp. 1829–1841. doi:10.1016/j.ijthermalsci.2009.02.009.

[5] Kremer, F., Schaub, J., Steffens, C., and Kolbech, A., 2012"Optimizing the noise of future passenger car diesel engines", MTZ, vol. 74, pp. 50-55.

[6] Ferrari, A., Mittica, A., and Spessa, E., 2013, "Benefits of hydraulic layout over driving system in piezo-injectors and proposal of a new-concept CR injector with an integrated Minirail", *Apply Energy*, vol. 103, pp. 243-255.

[7] Ferrari, A., Paolicelli, F., and Pizzo, P., 2015, "The new-generation of solenoid injectors equipped with pressure-balanced pilot valves for energy saving and dynamic response improvement"; *Applied Energy*, 151, pp. 367-376.

411 [8] d'Ambrosio, S., and Ferrari, A., 2014, "Potential of double pilot injection strategies optimized with a
412 design of experiments procedure in the improvement of diesel engine emissions and performance",
413 submitted to *Applied Energy*.

414 [9] Helmantel, J., Somhorst, J., and Denbratt, I., 2003, "Visualization of the effects of post injection and
415 swirl on the combustion process of a passenger car Common Rail DI diesel engine", ICES2003-622,
416 Proceeedings of the ASME conference, Salzbury.

417 [10] Chen, S. K., 2000, "Simultaneous reduction of NO_x and particulate emissions by using multiple
418 injections in a small engine", SAE Paper No.° 2000-01-3084.

419 [11] Surushima, T., Zhang, L., and Ishii, Y., 1999, "A study of unburned HC emission in small DI diesel
420 engines", SAE Paper No. 1999-01-0512.

421 [12] Dronniou, N., Lejeune, M., Balloul, I., and Higelin, P., 2005, "Combination of High EGR Rates and
422 Multiple Injection Strategies to Reduce Pollutant Emissions," SAE Paper No. 2005-01-3726, 2005.

423 [13] Zheng, Z., Lang, Y., Liu, H., Zhu, Y., Zhong, X., and Yao, M., 2015, "Effect of two-stage injection on
424 combustion and emissions under high EGR rate on a diesel engine by fueling blends of diesel/gasoline,
425 diesel/n-butanol, diesel/gasoline/n-butanol and pure diesel", *Energy Conversion and Management*, vol. 90,
426 pp. 1-11.

427 [14] Walker, L.C., et al., 2011, "Method and system for reducing turbo lag in an engine", US Patent
428 Application 11/464.888 (Navistar).

429 [15] Parks, J., Huff, S., Kass, M., Sorey, J., 2007, "Characterization of in-cylinder techniques for thermal
430 management of diesel aftertreatment", SAE Paper No. 2007-01-3997.

431 [16] Guo, G., Warner, J., Cavataio, G., Dobson, D., Badillo, E., and Lambert, C., 2010, "The development of
432 advanced urea-SCR systems for Tier 2 Bin 5 and beyond diesel vehicles", SAE Paper No. 2010-01-1183.

433 [17] Desantes, J. M., Arrègle, J., Lopez, J. J., and Garcia, A., 2007, "A comprehensive study of diesel
434 combustion and emissions with post injection", SAE Paper No. 2007-01-0915.

435 [18] Dieselnet website, since 1997, “Engine & emission technology online”, www.dieselnet.com.

436 [19] Han, Z., Uludogan, A., Hampson, G. J., Reitz, R. D., 1996, “Mechanism of soot and NO_x emission
437 reduction using multiple injection in a diesel engine”, SAE Paper No. 960633.

438 [20] Mendez, S., and Thirouard, S., 2008, “Using Multiple Injection Strategies in Diesel Combustion:
439 Potential to Improve Emissions, Noise and Fuel Economy Trade-off in Low *CR* engines”, SAE *Int. J. Fuels*
440 *Lubr.*, Vol. 1, Issue 1, pp. 662-674.

441 [21] Yun, H. H., Sellnau, M., Milovanovic, N., and Zuelch, S., 2008, “Development of premixed low-
442 temperature diesel combustion in a HSDI engine”, SAE Paper No. 2008-01-0639.

443 [22] Park, C., Kook, S., and Bae, C., 2004, “Effects of multiple injections in a HSDI diesel engine equipped
444 with Common Rail injection system”, SAE Paper No. 2004-01-0127.

445 [23] Arregle, J., Pastor, J. V., Lopez, J. J., and Garcia, A., 2008, “Insights on post injection-associated soot
446 emissions in direct injection strategies”, *Combustion and Flame*, 154, pp. 448-461.

447 [24] Bobba, M., and Musculus, M., 2010 “Effects of post injections on in-cylinder and exhaust soot for low-
448 temperature combustion in a heavy-duty diesel engine”, *SAE Int. J. Engines*, Vol. 3, issue 1, p. 497.

449 [25] Ojeda, W.D., Zoldak, P., Espinosa, R., and Kumar, R., 2009, “Development of a Fuel Injection Strategy
450 for Partially Premixed Compression Ignition Combustion,” *SAE Int. J. Engines* 2(1):1473-1488.

451 [26] Thurnheer T., Edenhauser D., Soltic P., Schreiber D., Kirchen P., and Sankowski A., 2011,
452 “Experimental investigation on different injection strategies in a heavy-duty diesel engine: Emissions and
453 loss analysis”, *Energy Conversion and Management*, 52, pp. 457–467.

454 [27] Lee, J. W., Choi, H., Hong, K., Lee, S., Yu, S., Choi, S.M., and Min, K.D., 2013, “Comparison of the
455 effects of multiple injection strategy on the emissions between moderate and heavy EGR rate conditions: part
456 2-post injections”, *Journal of Mechanical Science and Technology*, 27(7), pp. 2217-2223.

457 [28] Helmantel, A., and Golovitchev, 2009, “Injection strategy optimization for a light duty DI diesel engine
458 in medium load conditions with high EGR rates”, SAE Paper No. 2009-01-1441.

[29] Lee, J. W., Choi, H., Lee, S., Shin, S., Choi, S. M., Song, H., and Min, K. D., 2012, "Emission reduction by close post injection strategy with modified nozzle and piston bowl geometry at diesel combustion with heavy *EGR* rate", SAE Paper No. 2012-01-0681.

[30] Badami, M., Mallamo, F, and Millo, F., 2003, "Experimental investigation on the effect of multiple injection strategies on emissions, noise and brake specific fuel consumption of an automotive direct injection common-rail diesel engine"*, International journal of engine research* 4(4), pp. 299-314.

[31] Badami, M., Mallamo, F, and Millo, F., 2002, "Analysis of multiple injection strategies for the reduction of emissions, noise and bsfc of DI CR small displacement non-road diesel engine"*,* SAE Paper No. 2002-01-2672.

[32] Zheng Z., Yue L., Liu H., Zhu Y., Zhong X., and Yao M., 2015, "Effect of two-stage injection on combustion and emissions under high EGR rate on a diesel engine by fueling blends of diesel/gasoline, diesel/n-butanol, diesel/gasoline/n-butanol and pure diesel", *Energy Conversion and Management*, 90, pp. 1-15.

[33] Finesso, R., and Spessa, E, 2014, "A real time zero-dimensional diagnostic model for the calculation of in-cylinder temperatures, HRR and nitrogen oxides in diesel engines. *Energy Conversion and Management* 79 498–510. http://dx.doi.org/10.1016/j.enconman.2013.12.045.

[34] Akihama, K., Takatori, Y., Inagaki, K., Sakaki, S., and Dean, A. M., 2001, "Mechanism of smokeless rich diesel combustion by reducing temperature", SAE Paper No. 2001-01-0655.

[35] Mohan, B., Yang, W., and Chlu, S. K., 2013, "Fuel injection strategies for performance improvement and emission reduction in compression ignition engines - A review", *Renewable and Sustainable Energy Reviews*, 28, pp. 664-676.

[36] Lee, J. W., Choi, S. M., Shin, S. H., Choi, M., and Min, K. D., 2012, "Experimental analysis of emission reduction by the split injection strategy using close post injection with a double-row nozzle in heavy EGR conditions", *Journal of Mechanical Science and Technology*, 26(4), pp. 1-10.

483 [37] Zhuang J, Qiao X, Bai J, Hu Z, 2014, “Effect of injection-strategy on combustion, performance and
484 emission characteristics in a DI-diesel engine fueled with diesel from direct coal liquefaction”, *Fuel* 121 pp.
485 141–148. http://dx.doi.org/10.1016/j.fuel.2013.12.032.

486 [38] Gan S, Ng HK, Pang KM, 2011, “Homogeneous charge compression ignition (HCCI) combustion:
487 implementation and effects on pollutants in direct injection diesel engines”. *Applied Energy*;88(3):559–567.

488 [39] Priede, T., 1979, “Problems and Developments in Automotive Engine Noise Research," SAE Technical
489 Paper No. 790205.

490 [40] Busch, S., Zha, K., and Miles, P. C., 2014, “Investigations of closely coupled pilot and main injections
491 as a mean to reduce combustion noise”, Thiesel Conference, September 9th-12th, Valencia, Spain.

492 [41] Herfatmanesh M.R,. Lu P., Attar M.A., and Zhao H., 2013, “Experimental investigation into the effects
493 of two-stage injection on fuel injection quantity, combustion and emissions in a high-speed optical common
494 rail diesel engine”, *Fuel* 109 pp. 137–147. http://dx.doi.org/10.1016/j.fuel.2013.01.013.

495 [42] Baratta M., Catania A.E., Ferrari A., Finesso R. and Spessa E., 2011, “Premixed-Diffusive Multizone
496 Model for Combustion Diagnostics in Conventional and PCCI Diesel Engines”, *ASME Trans. Journal of*
497 *Engineering for Gas Turbines and Power*, vol. 133 n. 10, Art. No. 102801, pp. 1-13.

Engine type	2.0L Euro 5
Displacement	1956 cm^3
Bore × stroke	83.0 mm × 90.4 mm
Compression ratio	16.3
Valves per cylinder	4
Turbocharger	Twin-stage with valve actuators and WG
Fuel injection system	CR 2000 bar piezoelectric indirect acting injectors
Specific power and torque	71 kW/l – 205 Nm/l
EGR system type	Short-route cooled EGR

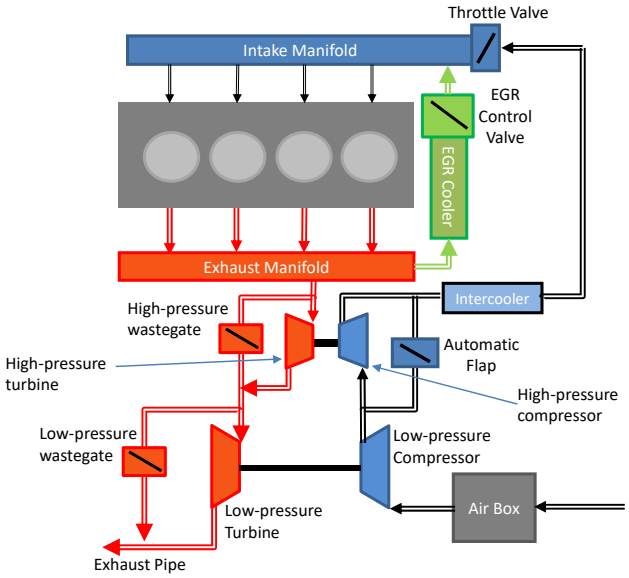

Table 1: Main specifications of the reference engine.

498

Quantity	Levels	Optimization
SOI_{Main} [°CA bTDC]	–3 –1 1	1
m_a [mm^3/(stk·cyl)]	360 380 390 400 420	384
Sw [%]	30 40 50	30
p_{Rail}[bar]	750 850 950 1050 1150	750
q_{Pil} [mm^3/(stk·cyl)]	0.8 1.1 1.4 1.7 2	1.42
DT_{Pil} [µs]	600 850 1100 1350 1600	600
q_{Afi} [mm^3/(stk·cyl)]	1 1.5 2 2.5 3	1
DT_{Afi} [µs]	600 933 1267 1600 1933 2267 2600	1082

Table 2: Levels considered for the variation list and optimized values of the inputs for the pMa injection strategy at 2000×5.

499

Quantity	Levels	Optimization
SOI_{Main} [°CA bTDC]	4 5 6 7 8	6.19
m_a [mm^3/(stk·cyl)]	680 690 700 710 720	720
Sw [%]	10 27.5 45	25
p_{Rail} [bar]	1500 1575 1650 1725 1800	1504.3
q_{Pil} [mm^3/(stk·cyl)]	0.7 1 1.3	0.7
DT_{Pil} [µs]	800 1000 1200 1400 1600	1600
q_{Aft} [mm^3/(stk·cyl)]	0.7 1.25 1.8 2.35 2.9 3.45 4	0.7
DT_{Aft} [µs]	800 950 1100 1250 1400	1203
p_{Boost} [mbar]	2200 2300 2400 2500 2600	2563

Table 3: Levels considered for the variation list and optimized values of the inputs for the pMa injection strategy at 2750×12.

500

501

Quantity	Levels	Optimal
SOI_{Main} [°CA bTDC]	–4 –2 0	0
m_a [mm³/(stk·cyl)]	340 357.5 392.5 410	358.1
Sw [%]	30 40 50	44
p_{Rail}[bar]	600 700 800 900 1000	620.1
q_{Pil1} [mm³/(stk·cyl)]	0.8 1.1 1.4 1.7 2	1
DT_{Pil1} [µs]	600 850 1100 1350 1600	905
q_{Pil2} [mm³/(stk·cyl)]	0.8 1.15 1.5	0.8
DT_{Pil2} [µs]	600 850 1100 1350 1600	614
q_{Aft} [mm³/(stk·cyl)]	0.8 1.35 1.9 2.45 3	0.8
DT_{Aft} [µs]	600 1000 1400 1800 2200 2600 3300	684

Table 4: Levels considered for the variation list and optimized values of the inputs for the ppMa injection strategy at 1500×5.

502

Strategy	NOx [g/kWh]	HC [g/kWh]	CO [g/kWh]	Soot [g/kWh]	bsfc [g/kWh]	CN [dBA]
pM	0.99	0.3	1.9	0.3	247	86.5
pMa	min	≤0.5	≤3	≤0.7	≤250	≤86.5

Table 5: Reference values of the reference *pM* calibration baseline point and constraints for the optimization of the *pMa* injection strategy at 2000×5.

503

Strategy	NO_x [g/kWh]	HC [g/kWh]	CO [g/kWh]	Soot [g/kWh]	bsfc [g/kWh]	CN [dBA]
pM	1.7	0.09	0.9	0.17	223	87.1
pMa	min	≤0.1	≤0.9	≤0.3	≤230	≤87.1

Table 6: Reference values of the reference pM calibration baseline point and constraints for the optimization of the *pMa* injection strategy at 2750×12.

504

Strategy	NOx [g/kWh]	HC [g/kWh]	CO [g/kWh]	Soot [g/kWh]	bsfc [g/kWh]	CN [dBA]
pM	0.89	0.33	1.8	0.17	235	80.5
ppMa	min	≤0.33	≤2	≤0.4	≤235	≤79

Table 7: Reference values of the reference *pM* calibration baseline point and constraints for the optimization of the *ppMa* injection strategy at 1500×5.

505

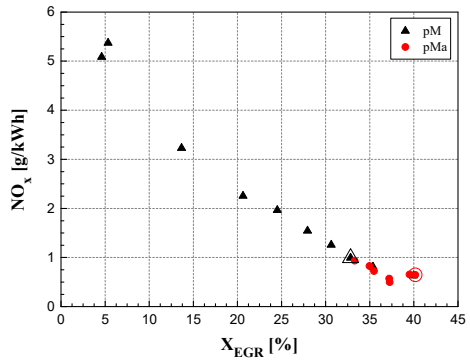

Figure 1. *NO_X-X_{EGR}* curve for the *pM* and *pMa* strategies (*bmep*=5 bar, *n*=2000 rpm).

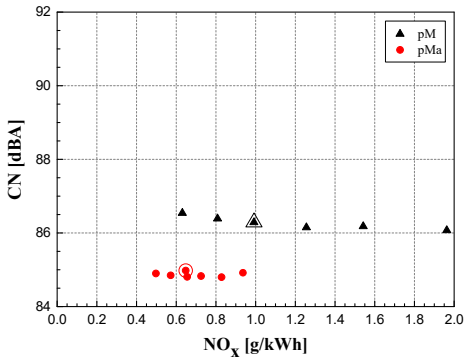

Figure 2. *CN-NO_X* trade-off for the *pM* and *pMa* strategies (*bmep*=5 bar, *n*=2000 rpm).

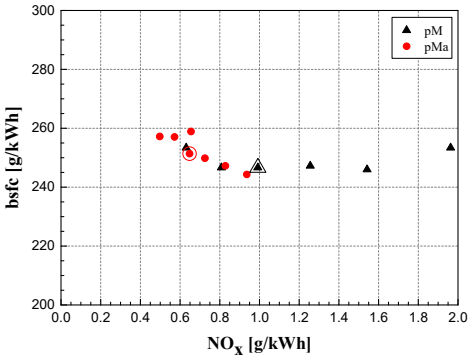

Figure 3. *bsfc-NO_X* trade-off for the *pM* and *pMa* strategies (*bmep*=5 bar, *n*=2000 rpm).

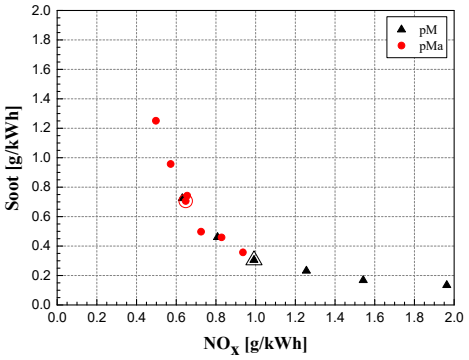

Figure 4. CO-*NO_X* trade-off for the *pM* and *pMa* strategies (*bmep*=5 bar, *n*=2000 rpm).

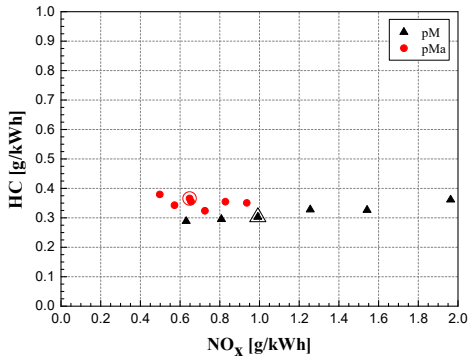

Figure 5. *HC-NO_X* trade-off for the *pM* and *pMa* strategies (*bmep*=5 bar, *n*=2000 rpm).

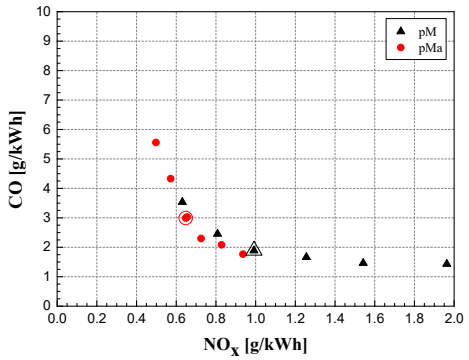

Figure 6. CO-*NO_X* trade-off for the *pM* and *pMa* strategies (*bmep*=5 bar, *n*=2000 rpm).

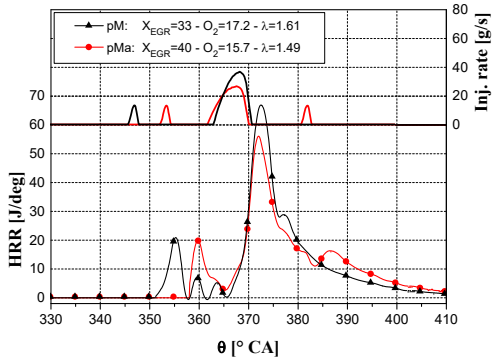

Figure 7. *HRR* versus *θ* distribution for the *pM* and *pMa* strategies (*bmep*=5 bar, *n*=2000 rpm).

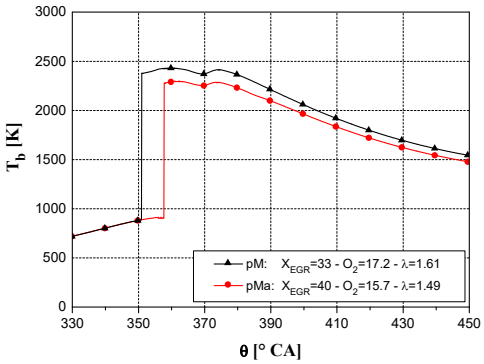

Figure 8. T_b versus *θ* distribution for the *pM* and *pMa* strategies (*bmep*=5 bar, *n*=2000 rpm).

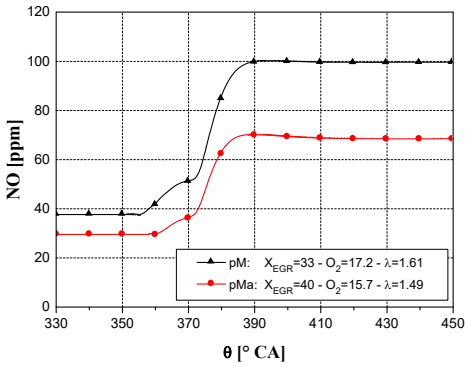

Figure 9. *NO* versus θ distribution for the *pM* and *pMa* strategies (*bmep*=5 bar, *n*=2000 rpm).

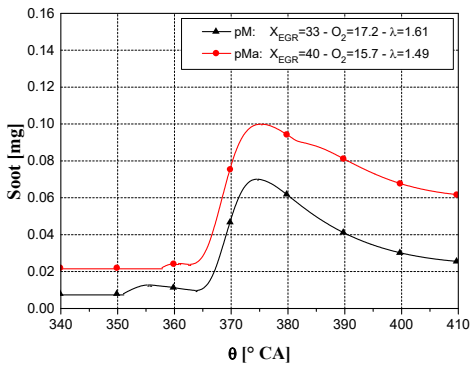

Figure 10. *PM* versus θ distribution for the *pM* and *pMa* strategies (*bmep*=5 bar, *n*=2000 rpm).

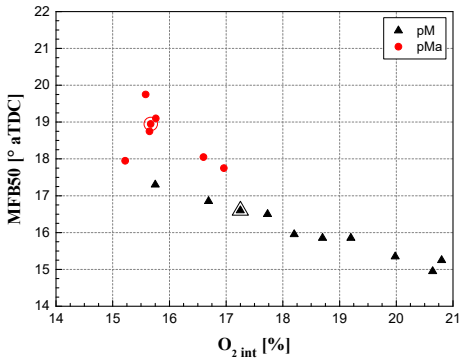

Figure 11. *MFB50* as a function of X_{EGR} for the *pM* and *pMa* strategies (*bmep*=5 bar, *n*=2000 rpm).

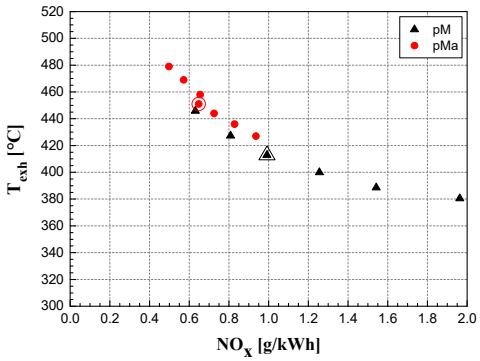

Figure 12. T_{exh} as a function of X_{EGR} for the *pM* and *pMa* strategies (*bmep*=5 bar, *n*=2000 rpm).

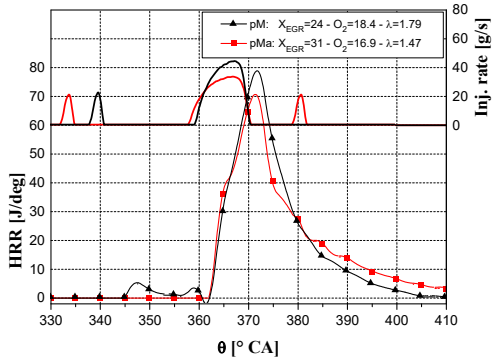

Figure 13. *HRR* versus θ distribution for the *pM* and *pMa* strategies (*bmep*=8 bar, *n*=2500 rpm).

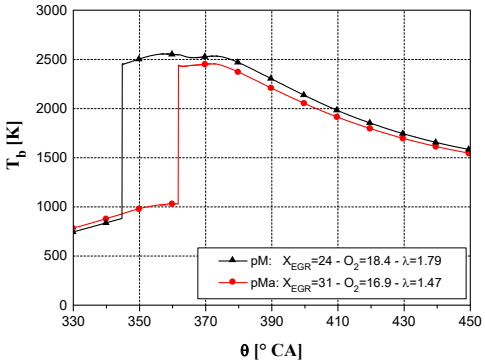

Figure 14. T_b versus θ distribution for the *pM* and *pMa* strategies (*bmep*=8 bar, *n*=2500 rpm).

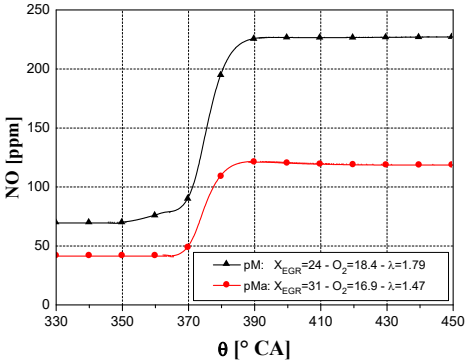

Figure 15. NO_x versus θ distribution for the *pM* and *pMa* strategies (*bmep*=8 bar, *n*=2500 rpm).

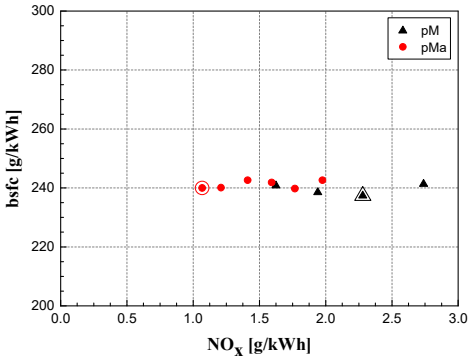

Figure 16. *bsfc*-NO_X trade-off for the *pM* and *pMa* strategies (*bmep*=8 bar, *n*=2500 rpm).

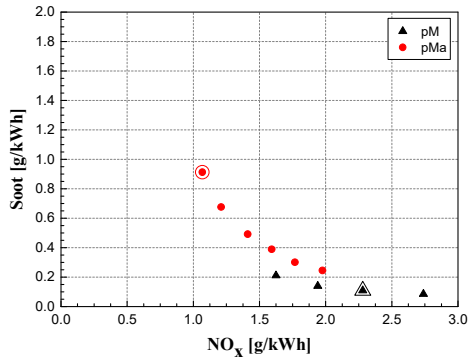

Figure 17. Soot-NO_X trade-off for the *pM* and *pMa* strategies (*bmep*=8 bar, *n*=2500 rpm).

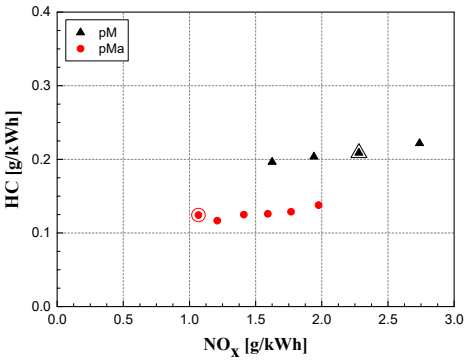

Figure 18. *HC-NO$_X$* curve for the *pM* and *pMa* strategies (*bmep*=8 bar, *n*=2500 rpm).

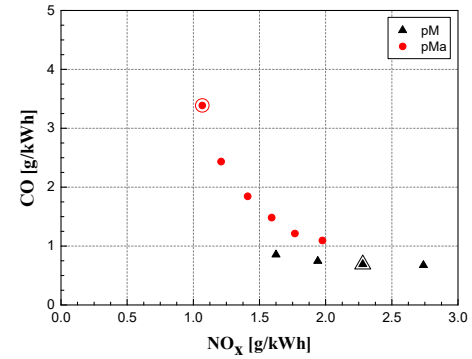

Figure 19. *CO-NO$_X$* trade-off for the *pM* and *pMa* strategies (*bmep*=8 bar, *n*=2500 rpm).

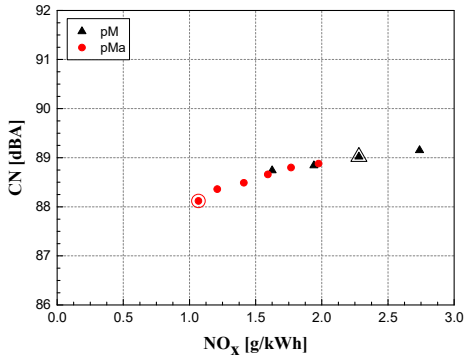

Figure 20. *CN-NO$_X$* curve for the *pM* and *pMa* strategies (*bmep*=8 bar, *n*=2500 rpm).

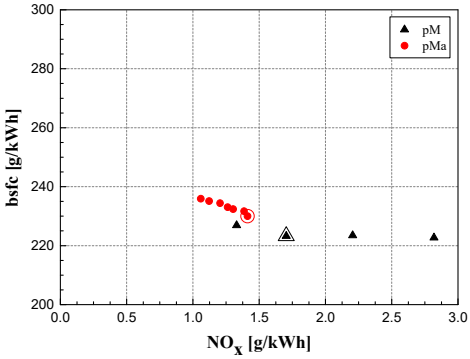

Figure 21. *bsfc-NO$_x$* trade-off for the *pM* and *pMa* strategies (*bmep*=12 bar, *n*=2750 rpm).

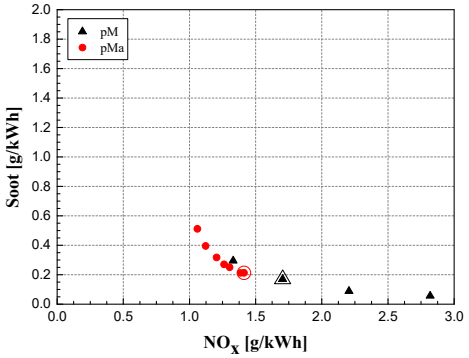

Figure 22. Soot-*NO$_X$* trade-off for the *pM* and *pMa* strategies (*bmep*=12 bar, *n*=2750 rpm).

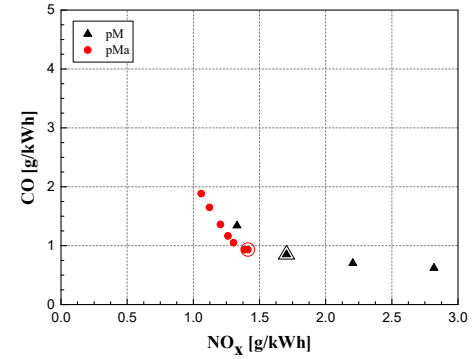

Figure 23. CO-*NO$_X$* trade-off for the *pM* and *pMa* strategies (*bmep*=12 bar, *n*=2750 rpm).

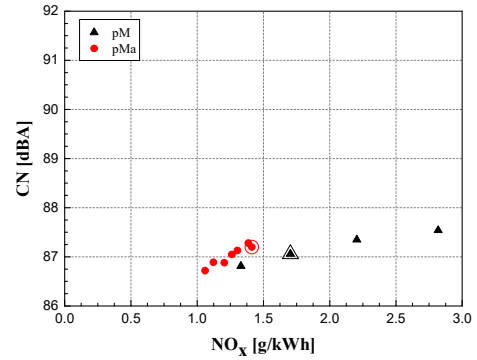

Figure 24. *CN-NO$_X$* curve for the *pM* and *pMa* strategies (*bmep*=12 bar, *n*=2750 rpm).

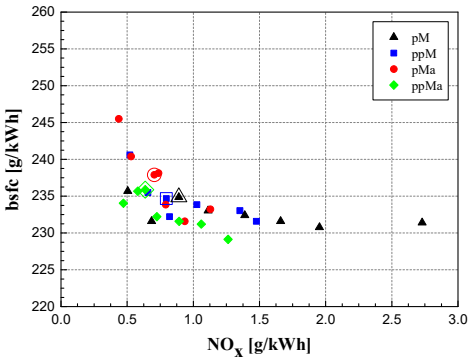

Figure 25. *bsfc*-NO_X trade-off for the *pM*, *ppM*, *pMa* and *ppMa* strategies (*bmep*=5 bar, *n*=1500 rpm).

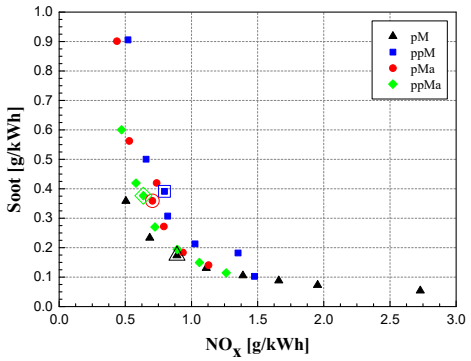

Figure 26. Soot-NO_X trade-off for the *pM*, *ppM*, *pMa* and *ppMa* strategies (*bmep*=5 bar, *n*=1500 rpm).

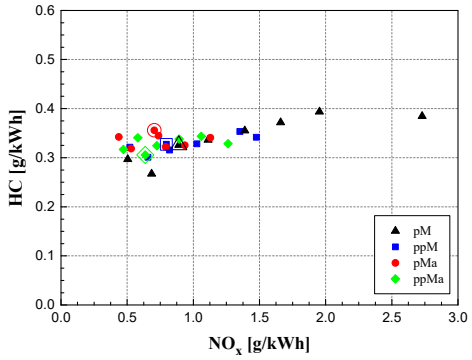

Figure 27. *HC*-NO_X trade-off for the *pM*, *ppM*, *pMa* and *ppMa* strategies (*bmep*=5 bar, *n*=1500 rpm).

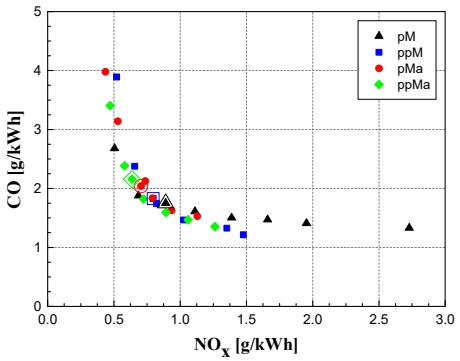

Figure 28. *CO*-NO_X trade-off for the *pM*, *ppM*, *pMa* and *ppMa* strategies (*bmep*=5 bar, *n*=1500 rpm).

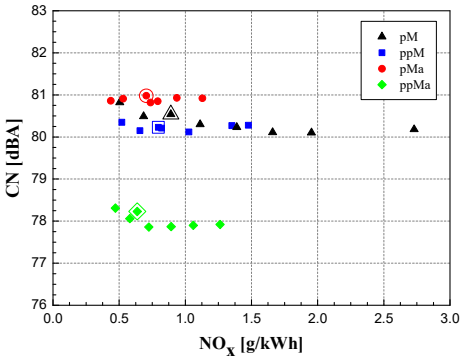

Figure 29. *CN*-NO_X curve for the *pM*, *ppM*, *pMa* and *ppMa* strategies (*bmep*=5 bar, *n*=1500 rpm).

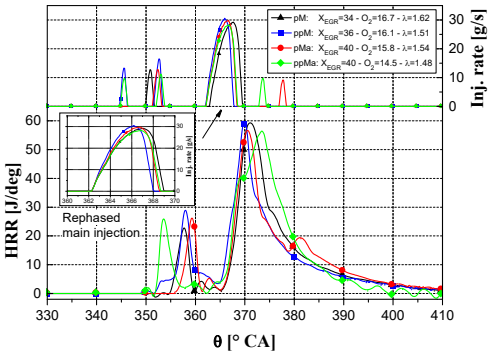

Figure 30. *HRR* versus θ distribution for the *pM*, *ppM*, *pMa* and *ppMa* strategies (*bmep*=5 bar, *n*=1500 rpm).

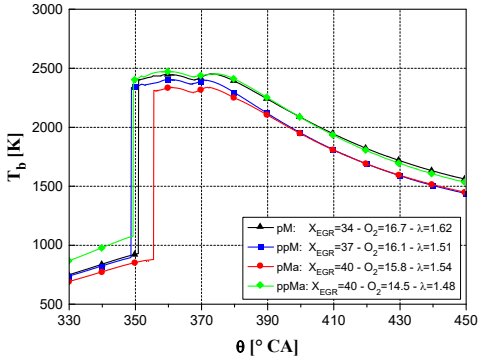

Figure 31. T_b versus θ distribution for the *pM*, *ppM*, *pMa* and *ppMa* strategies (*bmep*=5 bar, *n*=1500 rpm).

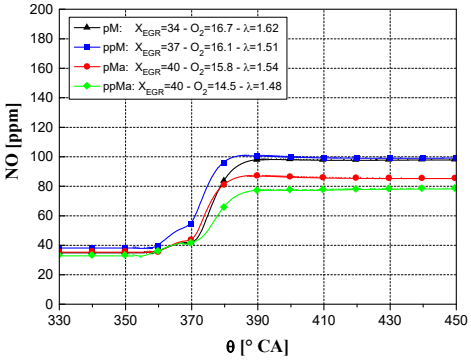

Figure 32. NO_x versus θ distribution for the *pM*, *ppM*, *pMa* and *ppMa* strategies (*bmep*=5 bar, *n*=1500 rpm).

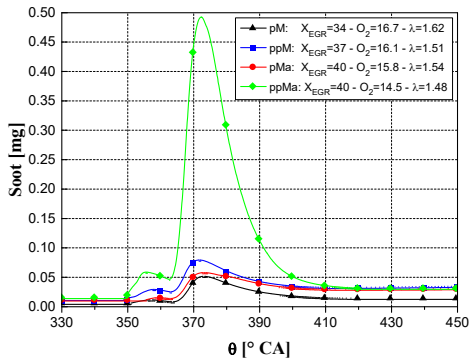

Figure 33. Soot versus θ distribution for the *pM*, *ppM*, *pMa* and *ppMa* strategies (*bmep*=5 bar, *n*=1500 rpm).